


High-pressure methane adsorption behavior on deep shales: Experiments and modeling

Cite as: Phys. Fluids **33**, 063103 (2021); <https://doi.org/10.1063/5.0054486>

Submitted: 19 April 2021 • Accepted: 20 May 2021 • Published Online: 04 June 2021

 Weijun Shen (沈伟军), Xizhe Li (李熙喆), Tianran Ma (马天然), et al.



View Online



Export Citation



CrossMark

ARTICLES YOU MAY BE INTERESTED IN

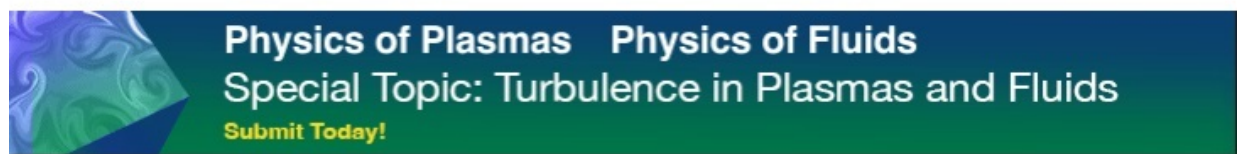
[Spontaneous imbibition in tight porous media with different wettability: Pore-scale simulation](#)
Physics of Fluids **33**, 032013 (2021); <https://doi.org/10.1063/5.0042606>

[High resolution crossed molecular beams study of the \$H+HD\rightarrow H_2+D\$ reaction](#)

Chinese Journal of Chemical Physics **32**, 123 (2019); <https://doi.org/10.1063/1674-0068/cjcp1901010>

[Modeling quasi-3D needle-punched C/C composites using a linear simplification representative volume element model](#)

AIP Advances **9**, 035344 (2019); <https://doi.org/10.1063/1.5068727>



High-pressure methane adsorption behavior on deep shales: Experiments and modeling

Cite as: Phys. Fluids **33**, 063103 (2021); doi: [10.1063/5.0054486](https://doi.org/10.1063/5.0054486)

Submitted: 19 April 2021 · Accepted: 20 May 2021 ·

Published Online: 4 June 2021





View Online



Export Citation



CrossMark

Weijun Shen (沈伟军),^{1,2,3,a)}  Xizhe Li (李熙喆),⁴⁾ Tianran Ma (马天然),⁵⁾ Jianchao Cai (蔡建超),⁶⁾ 
Xiaobing Lu (鲁晓兵),^{1,3)} and Shangwen Zhou (周尚文)⁴⁾

AFFILIATIONS

¹⁾Key Laboratory for Mechanics in Fluid Solid Coupling Systems, Institute of Mechanics, Chinese Academy of Sciences, Beijing 100190, China

²⁾State Key Laboratory of Oil and Gas Reservoir Geology and Exploitation, Southwest Petroleum University, Chengdu, Sichuan 610500, China

³⁾School of Engineering Science, University of Chinese Academy of Sciences, Beijing 100049, China

⁴⁾PetroChina Research Institute of Petroleum Exploration and Development, Beijing 10083, China

⁵⁾School of Mechanics and Civil Engineering, China University of Mining and Technology, Xuzhou, Jiangsu 221116, China

⁶⁾State Key Laboratory of Petroleum Resources and Prospecting, China University of Petroleum, Beijing 102249, China

^{a)}Author to whom correspondence should be addressed: wjshen763@imech.ac.cn

ABSTRACT

Understanding methane adsorption behavior on deep shales is crucial for estimating the original gas in place and enhancing gas recovery in deep shale gas formations. In this study, the methane adsorption on deep shales within the lower Silurian Longmaxi formation from the Sichuan Basin, South China was conducted at pressures up to 50 MPa. The effects of total organic carbon (TOC), temperatures, clay minerals, and moisture content on the adsorption capacity were discussed. The results indicated that the methane excess adsorption on deep shales increased, then reached its peak, and finally decreased with the pressure. The excess adsorption data were fitted using the adsorption models, and it was found that the Dubinin–Radushkevich (D–R) model was superior to other models in predicting the methane adsorption behavior. The methane adsorption capacities exhibited strong positive correlations with the TOC content and negative relationships with clay minerals. The methane excess adsorption decreased with the temperature, while the opposite trend would occur once it exceeded some pressure. The presence of the moisture content on deep shales sharply decreased the methane adsorption capacities, and the reduction of the adsorption capacity decreased with the pressure. The moisture would occupy the adsorption sites in the shale pores, which could result in the methane adsorption capacity that decreased.

Published under an exclusive license by AIP Publishing. <https://doi.org/10.1063/5.0054486>

I. INTRODUCTION

With the increasing demand for natural gas resources in China, shale gas is the most important field to realize the rapid production of natural gas from now on.^{1,2} Deep shale gas resources in China are abundant and owning an immense potential for exploitation, which is becoming a key area for shale gas production in the future. According to the statistics, shale gas resources of China in place are estimated to $144.5 \times 10^{12} \text{ m}^3$ and the recoverable resources are $36.1 \times 10^{12} \text{ m}^3$, respectively, while the deep shale gas resources buried below 3500 m account for more than 65%.³ The Sichuan Basin is one of the major shale-gas-producing areas in China, and the shale gas resources at the depth of no more than 4500 m are $16.3 \times 10^{12} \text{ m}^3$, including $11.2 \times 10^{12} \text{ m}^3$ at the depth of more than 3500 m, which are mainly

distributed in the southeast, south, and north of Sichuan.^{3,4} The deep shale gas formations are characterized by high pressure, high *in situ* stress, and strong plasticity, and there exist some difficulties in well completions and volume fracturing in horizontal wells for shale gas.^{5,6} Therefore, accelerating the exploration and development of deep shale gas resources is of great strategic significance for relieving the contradiction between supply and demand of natural gas in China and optimizing energy structure.

Compared with conventional gas reservoirs, the shale gas reservoir itself was both the generating source and the storing place of shale gas.⁷ Generally, there existed three types of stored shale gas in the shale formation: free gas in fractures and pores, adsorbed gas on organic matter and clay minerals, and dissolved gas in the liquid hydrocarbon

and water.^{8,9} The total shale gas-in-place (GIP) estimated by summing these three components was an important parameter for the economic assessment in shale gas formations. Ambrose *et al.*¹⁰ suggested that the contribution of adsorbed gas to the total GIP in shales was as much as 20%–85% in shale gas formations. Consequently, understanding the methane adsorption behavior in shales is essential for the accurate assessment of shale gas formations. In recent years, there were a large number of experimental studies on methane adsorption in shales. Rexer *et al.*¹¹ studied the methane adsorption on a dry, organic-rich Alum shale sample at pressures up to 14 MPa. Merkel *et al.*¹² observed the dry and moisture-equilibrated shale samples from the Midland Valley Basin, Scotland at 45 °C and up to 25 MPa. Jiang *et al.*¹³ measured the methane adsorption capacity on terrestrial shale from the Yanchang formation in the Ordos Basin, China under geological conditions up to 25 MPa and 70 °C. Wang *et al.*¹⁴ performed methane adsorption experiments at pressures up to 12 MPa and 313 K on dry and moisture-equilibrated shales from the Qaidam Basin, China. Qi *et al.*¹⁵ measured methane adsorption isotherms between 30 °C and 80 °C for pressures up to 20 MPa for three shale samples from Sichuan Basin in China. Hu and Mischo¹⁶ conducted methane adsorption capacities on shales in the South China between 40 °C and 100 °C at 30 MPa. However, the maximum pressure of the above investigations on methane adsorption was less than 40 MPa, which was far below the reservoir pressure of deep shale formations. Since the deep shale formations are buried at a depth of more than 3500 m, the reservoir pressure of practical shale formations exceeds 40 MPa.¹⁷ The detailed methane adsorption characteristics in deep shale gas reservoirs under high pressure are lacking and many uncertainties exist in the process. Therefore, it is extremely necessary to understand the behavior of high-pressure methane adsorption on deep shales so as to estimate the shale GIP and enhance gas productivity in deep shale formations.

Many adsorption theories and models have been developed to characterize and understand the methane adsorption behavior for shale gas reservoirs. The classical Langmuir model was mainly used to fit the adsorption isotherm data, and then can calculate the shale-adsorbed gas under shale reservoir conditions.¹⁸ However, many scholars have found that the Langmuir model could not always well describe the adsorption behavior in deep shales under the high-pressure conditions.^{19,20} The main reason was that the critical temperature and pressure of methane are −82.5 °C and 4.59 MPa, respectively, and the methane adsorption in shales was supercritical under shale formation conditions.²¹ Considering the supercritical adsorption characteristics, some supercritical adsorption models have been proposed to describe the high-pressure adsorption in shales, including modified-Langmuir (M-L), Langmuir–Freundlich (L-F), simplified local-density (SLD), Dubinin–Radushkevich (D-R), and Dubinin–Astakhov (D-A) models.^{22–25} Zhou *et al.*²² suggested that the methane adsorbed on shales can be estimated more reliably using the D-R model than the M-L model. Chareonsuppanimit *et al.*²⁴ indicated that the SLD was used to describe the high-pressure adsorption behavior on shales, and there existed the experimental uncertainties in gas-specific and adsorbent-specific parameters. Li *et al.*²⁶ considered that the M-L model, the L-F model, and the D-A model all had their advantages, and their calculated values were well consistent with the measured data. It can be argued that the determination of methane adsorption model adsorption on shales under high pressure is challenging, and many uncertainties still exist in the process. Therefore, it

is extremely necessary to determine the adsorption model on shales under the high-pressure condition so as to understand supercritical methane adsorption of shales in shale reservoir formations.

In this study, the high-pressure methane adsorption on deep shales from the lower Silurian Longmaxi formation in the Sichuan Basin, South China was performed using the volumetric method under different temperatures and at pressure up to 50 MPa. The high-pressure methane adsorption behavior of deep shales was analyzed and the excess/absolute adsorption was discussed. Four common adsorption models were used to fit the experimental data and illustrate the adsorption isotherms, including the M-L, L-F, D-R, and D-A models. Furthermore, the effects of temperatures, clay minerals, and moisture on high-pressure methane adsorption on deep shales were investigated, respectively.

II. EXPERIMENTAL MATERIALS AND METHODS

A. Shale samples

Six shale samples used in this study were obtained from different sites within the lower Silurian Longmaxi formation from the Sichuan Basin, South China, which ranged from 3873.92 to 4035.89 m, and these deep shales are illustrated in Fig. 1. The lower Silurian Longmaxi formation in the Weiyuan and Changning area was dominated by black argillaceous shales with a stable thickness between 10 and 60 m, which was composed of the lower member and the upper member.²⁷ The vitrinite reflectance varies from 2.3% to 2.8% and the total organic carbon (TOC) content ranges from 2% to 6%. Before the measurements, all the shale samples were crushed into the 40–100 mesh size powder and sieved to select different grain sizes. The different grain-size shale samples were first placed in a drying oven at 105 °C (24 h), and then cooled to room temperature in a vacuum desiccator. Parts of grain-size shale samples were used for the shale chemical–physical characterization, and others were used for the high-pressure methane adsorption.

B. Measurements and experiments

To determine the TOC contents, the shale samples were crushed to pass through the <250 μm sieve. The TOC and total inorganic carbon (TIC) analyses were then measured on the <250 μm shale sample's fraction with a Shimadzu TOC-VCPH. The x-ray diffraction (XRD) was obtained using a Bruker D8 ADVANCE diffractometer with Cu Kα x-rays (1.5406 Å) at 40 kV and 40 mA. The 2θ scan range was between 3° and 45° with a step size of 0.02° and an increased rate of 2°/min. The pore size distribution of the shales was achieved using low-pressure N₂ adsorption/desorption at 77 K with a relative pressure (P/P_0) between 0.01 and 0.995 on a porosimetry system (NOVA3200e, Quantachrome USA). Each shale sample was crushed and sieved to selected the 250–500 μm and then outgassed at 110 °C for 24 h to remove bound water and residual gases. The N₂ adsorption data from $P/P_0 = 0.05$ –0.35 were selected to determine the specific surface area (S_{BET}) with the Brunauer–Emmett–Teller (BET) method.²⁸ The total pore volume (V) was obtained at a relative pressure of 0.995, and the average pore diameter was determined from $4V/S_{BET}$.²⁹

The methane adsorption measurements were carried out on the shale samples with a 3H-2000PH adsorption equipment at pressures up to 51 MPa and temperatures of 313 and 333 K, and the schematic diagram of the equipment is illustrated in Fig. 2. In this study, the methane adsorption experiments were conducted on the crushed shale

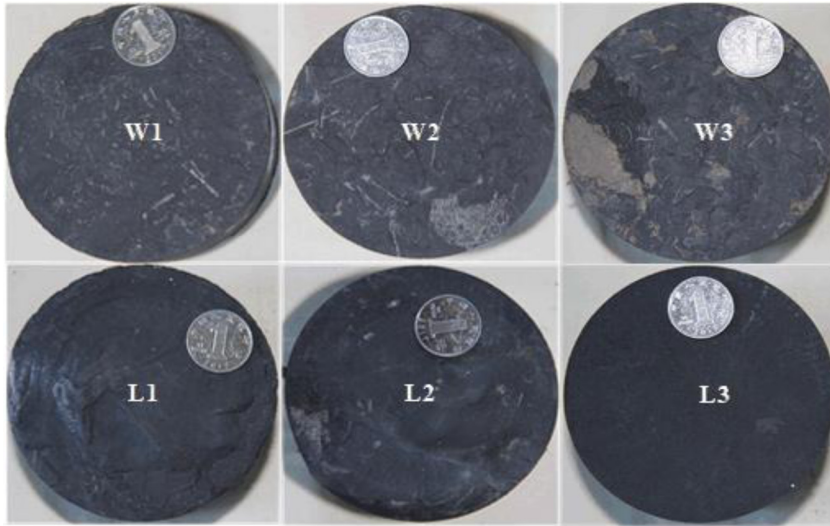


FIG. 1. Deep shales from various sites within the lower Silurian Longmaxi formation.

samples with the grain sizes from 40 to 100 mesh at 313 K. Approximately 130 g of the crushed shale samples was used for each experiment, and the high-purity (99.99%) methane was injected in the experiments. The first point was the vacuum and the equilibrium time of each pressure point less than 10 MPa was set as 2 h, while the equilibrium time of each pressure point more than 10 MPa was 4 h so as to ensure the pressure stability in the methane adsorption. The highest experimental pressure point was about 50 MPa and there were more than 10 experimental data points. After the experiment at 313 K was completed, the experiment of methane adsorption on the shale samples at 333 K was performed. To evaluate the experimental repeatability, the methane adsorption measurement was repeated on the wet condition at 333 K for each sample.

III. MODELING

A. Excess and absolute adsorption

Since the critical temperature and pressure of methane are -82.5°C and 4.59 MPa, respectively, the methane adsorption on deep shales was supercritical when they exceeded the critical state. On the conditions of the experimental pressure and temperature, the adsorption amount measured is the so-called excess adsorption amount, and the excess adsorption amount is significantly smaller than the corresponding absolute adsorption amount.^{30,31} The absolute adsorption amount of methane can be written as a function of the excess adsorption amount as

$$n_{ab} = n_{ex} / (1 - \rho_g / \rho_a), \tag{1}$$

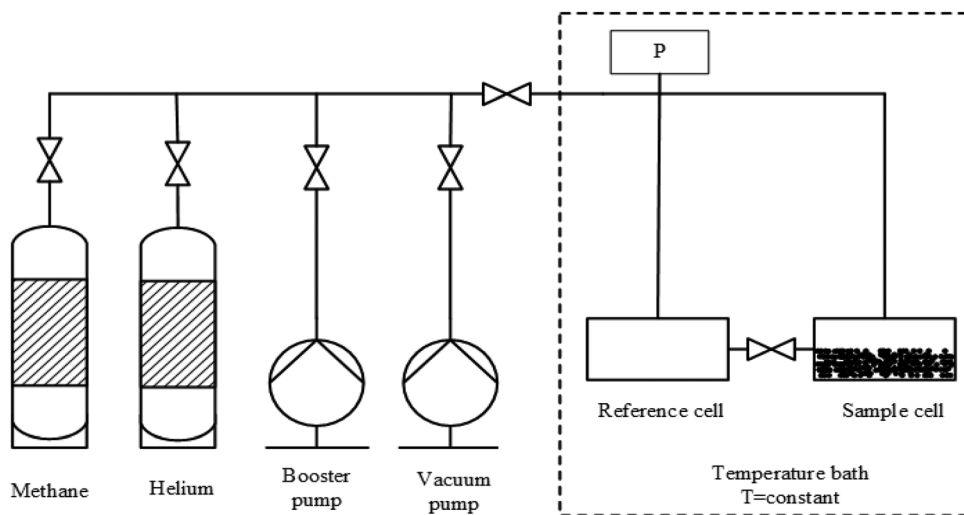


FIG. 2. Schematic diagram of the high-pressure methane adsorption on deep shales.

where n_{ab} and n_{ex} are the absolute and excess adsorption amounts, respectively; ρ_g is the bulk gas density of methane, which can be obtained from the Soave-Redlich-Kwong equation;³² and ρ_a is the adsorbed gas density of methane.

B. Adsorption models

1. Modified-Langmuir (M-L) model

Based on the assumptions that a monolayer of adsorbate occurs on the specific homogeneous sites of the solid adsorbent, the Langmuir adsorption model proposed by Langmuir was used to describe the gas and vapor adsorption in microporous solids.³³ The Langmuir adsorption model can be expressed as follows:

$$n_{ab} = \frac{n_L P}{P_L + P}, \quad (2)$$

where n_L is the maximum absolute amount of the monolayer adsorption; p and p_L are the adsorption pressure and the Langmuir pressure, respectively; and the remaining parameters are the same as above.

According to the definition of Gibbs adsorption,¹¹ the M-L excess adsorption model can be written as follows:

$$n_{ex} = \frac{n_L P}{P_L + P} (1 - \rho_g / \rho_a). \quad (3)$$

2. Langmuir-Freundlich (L-F) model

Considering the heterogeneity of adsorption sites in the adsorbents, Sips³⁴ proposed the L-F model extended from the Langmuir model, and the L-F adsorption model can be described as follows:

$$n_{ab} = \frac{n_L (bp)^m}{1 + (bp)^m}, \quad (4)$$

where b is the Langmuir pressure constant, m is the coefficient of adsorption uniformity, and the remaining parameters are the same as above.

By substituting Eq. (4) into Eq. (1), the L-F excess adsorption model can be written as follows:

$$n_{ex} = \frac{n_L (bp)^m}{1 + (bp)^m} (1 - \rho_g / \rho_a). \quad (5)$$

3. Dubinin-Radushkevich (D-R) model

On the basis of the Polanyi adsorption potential theory, the D-R model developed by Dubinin was used to qualify gas adsorption on microporous solids, which has been widely applied to characterize the micropore-rich materials.^{35,36} The D-R adsorption model can be expressed as follows:

$$n_{ab} = n_0 \exp \left\{ -D \left[\ln \left(\frac{\rho_a}{\rho_g} \right) \right]^2 \right\}, \quad (6)$$

where n_0 is the maximum absolute adsorption amount, D is the pore structure parameter, and the remaining parameters are the same as above.

By substituting Eq. (6) into Eq. (1), the D-R excess adsorption model can be written as follows:

$$n_{ex} = n_0 \exp \left\{ -D \left[\ln \left(\frac{\rho_a}{\rho_g} \right) \right]^2 \right\} (1 - \rho_g / \rho_a). \quad (7)$$

4. Dubinin-Astakhov (D-A) model

On the basis of the adsorption potential theory, the D-A model was proposed by Dubinin and Astakhov to model Type I adsorption isotherms, which provided an appropriate description of the adsorption phenomena occurring in the micropores.³⁷ The D-A adsorption model can be expressed as follows:

$$n_{ab} = n_0 \exp \left\{ -D \left[\ln \left(\frac{\rho_a}{\rho_g} \right) \right]^k \right\}, \quad (8)$$

where k is the structural heterogeneity parameter and the remaining parameters are the same as above.

By substituting Eq. (8) into Eq. (1), the D-A excess adsorption model can be written as follows:

$$n_{ex} = n_0 \exp \left\{ -D \left[\ln \left(\frac{\rho_a}{\rho_g} \right) \right]^k \right\} (1 - \rho_g / \rho_a). \quad (9)$$

IV. RESULTS AND DISCUSSION

A. Characterization of shale properties

The burial depth of these deep shale samples is over 3500 m, where the maturity of the gas shale reaches the overmature stage. The TOC content of the deep shales is summarized in Table I, which ranges from 0.2% to 4.5%, and the results implied that all the shales had the good kerogen quality except in sample W1.³⁸ The mineralogical composition of the studied deep shale samples is listed in Table II. These results indicated that the mineral composition of the lower Silurian Longmaxi formation from the Sichuan Basin was dominated by siliceous minerals (quartz and feldspar), clay minerals (illite, kaoline, and chlorite), and carbonatites (calcite and dolomite). The proportion of siliceous minerals was between 15.8% and 58.8%, and the most abundant siliceous mineral was quartz, which varies from 10.3% to 56.5%. The carbonatite content of these shales was between 2.5% and 11.3%. All these deep shales contained a minor pyrite with the content range from 2.3% to 6.1%, which indicated that there existed a reducing depositional environment. The pore-size distribution from low-pressure nitrogen adsorption data for deep shales is presented in Fig. 3, and all the deep shale samples showed a broad pore diameter range, with the majority of pores range from 1 nm to 100 nm. According to the International Union of Pure and Applied Chemistry (IUPAC) classification, the low-pressure nitrogen sorption behavior of these shale samples exhibited Type II isotherms.³⁹ These types of isotherms were common in the mesoporous materials, which illustrated the pore filling of micropores at lower relative pressures and multilayer adsorption at moderate pressures. When the relative pressure approximated 1, the sharp increase in the adsorbed amount suggested that there existed the macropores. The pore parameters for low-pressure nitrogen adsorption and desorption are shown in Table I. The BET-specific surface areas of all deep shales were between

TABLE I. Some measured characteristics of shale samples used in this study.

No.	Depth (m)	TOC (%)	Specific surface area (m ² /g)	Pore diameter (nm)
W1	3 873.92–3 874.00	1.08	16.43	4.66
W2	3 882.12–3 882.19	4.50	25.05	7.60
W3	3 886.66–3 886.73	3.39	24.75	8.91
L1	4 005.36–4 005.43	3.42	28.22	3.51
L2	4 008.53–4 008.60	0.20	11.03	3.64
L3	4 014.87–4 014.96	2.43	25.54	3.88

TABLE II. Major mineralogical composition of shale samples based on XRD analysis (%).

No.	Quartz	Illite	Chlorite	Calcite	Dolomite	Pyrite	Kaolinite	Feldspar
W1	33.3	27.6	17.7	1.4	1.1	6.1	7.6	5.2
W2	49	22.9	9.4	4.4	4.1	2.8	4.7	2.7
W3	42.7	24.3	12.5	3.3	3.1	2.3	7.4	4.4
L1	56.5	18.1	9.1	2.7	2.6	2.6	6.1	2.3
L2	10.3	72	0	1.4	1.4	2.6	6.8	5.5
L3	50	16.8	10.7	5.8	5.5	2.3	6.1	2.8

16.43 and 28.22 m²/g, and the average pore diameters were in the mesopore range, which varied from 3.51 to 8.91 nm.

B. High-pressure methane adsorption isotherms

The measured excess adsorption isotherms of all deep shale samples at the temperature of 313 K are shown in Fig. 4. As can be seen from Fig. 4, the excess adsorption isotherms of these deep shales had similar variation trends. The methane isothermal adsorption curves increased and then decreased with the increase in pressures, which represented an upper limit for methane adsorption. When the pressure was low less than 13 MPa, the methane adsorption capacity

increased with pressures and the isothermal adsorption curve increases rapidly, which showed a nearly linear growth. While the adsorption reached the high-pressure stage of more than 13 MPa, the methane molecules in the adsorption layers gradually increased to saturation, and the excess adsorption capacity gradually decreased with the increase in pressures. As illustrated in Fig. 4, all the maximum excess adsorbed amounts of the deep shales in this study showed good linear positive correlations with the TOC content, which implied that organic matter is the main supporting medium of methane molecules adsorbed in shales. It has been mentioned that a higher TOC content would result in a larger methane adsorption capacity.^{40,41} This phenomenon can be explained from the following two aspects. On the

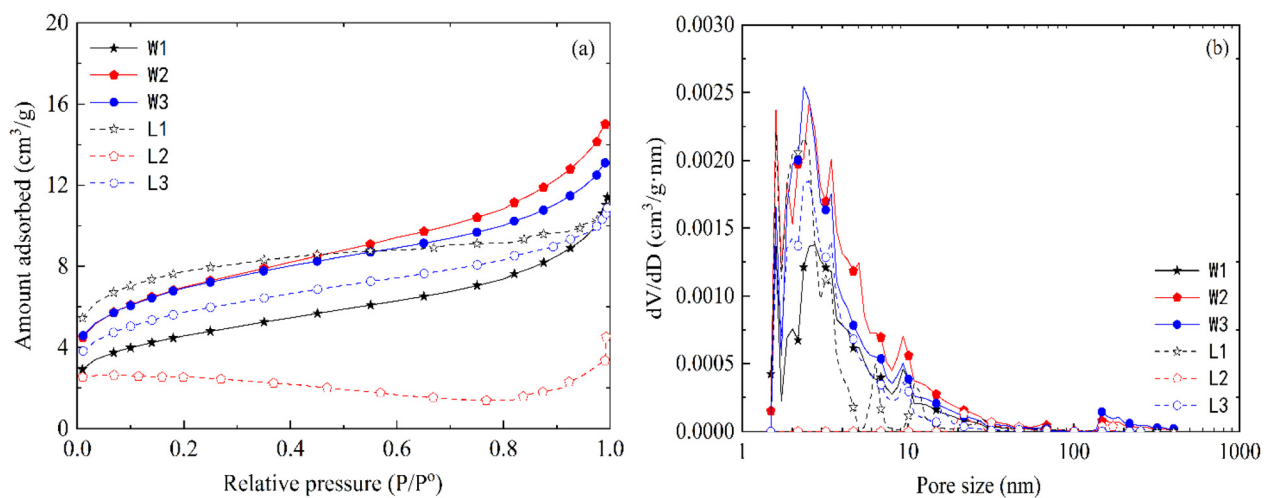


FIG. 3. Pore-size distribution from low-pressure nitrogen sorption data for deep shales: (a) low-pressure nitrogen sorption isotherms and (b) pore-size distribution.

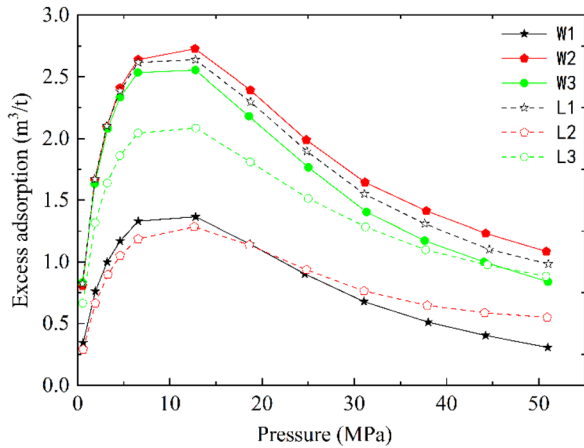


FIG. 4. Excess adsorption vs pressure on deep shales at 313 K.

one hand, extensive micro- and mesopores were widely observed in organic matter by low-pressure nitrogen sorption data. The extensive micro- and mesopores could provide large specific surface area and much sorption sites for methane molecules in deep shales. As a result of the higher density of the adsorbed phase, micro- and fine-mesopores would have great higher adsorption potentials than large meso-macropores in deep shales. Consequently, the methane molecules could occupy higher potential sites at the initial moment of the methane adsorption process. On the other hand, methane is a nonpolar gas, and methane molecules would be preferentially attracted by hydrophobic organic matter rather than other hydrophilic minerals.¹⁶ Therefore, the excess adsorption isotherms of these deep shale samples exhibited similar characteristics to the TOC contents, and their adsorption capacities would increase with the increasing TOC contents.

According to Eq. (4), the absolute adsorption amounts in deep shales under different pressures can be obtained, as illustrated in Fig. 5. As can be seen from Fig. 5, the absolute adsorption amounts of methane in deep shales showed similar variation characteristics, which

was a rapid increase trend and a slight change trend with increasing pressures. According to the IUPAC classification, the absolute adsorption behavior of these shale samples exhibited Type I isotherm.³⁹ At the low pressure (0–4 MPa), the absolute adsorption amount was almost as much as the excess adsorption amount. The main reason was that the gas volume phase density was relatively small at the low gas pressure, and the volume in the adsorption phase could be negligible.⁴² With the increasing gas pressure, the absolute adsorption of methane was inclined to increase while the excess adsorption gradually became parabolic. At the low, middle, and high pressures, the excess adsorption of methane in deep shales increased rapidly, then came to its peak, and finally decreased under high-pressure conditions. Since the large initial reservoir pressure of methane in deep shale formations, if the excess adsorption curve of methane at the low pressure was used for evaluating directly the adsorption ability in shale gas formations, and it would result in underestimating its actual adsorption capacity.

C. Data fitting of methane adsorption isotherms

The adsorption isotherms illustrate the relationship between the amounts of adsorbate adsorbed onto an adsorbent with a pressure change at a constant temperature.^{39,43} In order to describe the adsorption isotherm phenomenon, lots of adsorption isotherm models have been proposed and developed over the years.²⁵ As mentioned above, the excess adsorption isotherms of the deep shales were obtained from the measured data fitted using the previously described adsorption models, including the M-L, L-F, D-R, and D-A models. Figure 6 shows the comparisons between the measured data and different adsorption models on the deep shale samples W1 and L1. From the results of Fig. 6, all the adsorption models (M-L, L-F, D-R, and D-A) gave a good description of the measured data on the whole, and their corresponding average relative errors (AREs) were less than 5%, as summarized in Table III. Compared with these adsorption models, the D-R model was optimal to fit the high-pressure methane adsorption on deep shale samples, since it had the smallest ARE value in the whole pressure. The D-R model has been widely used to describe gas adsorption behavior on the micropore-rich materials in previous

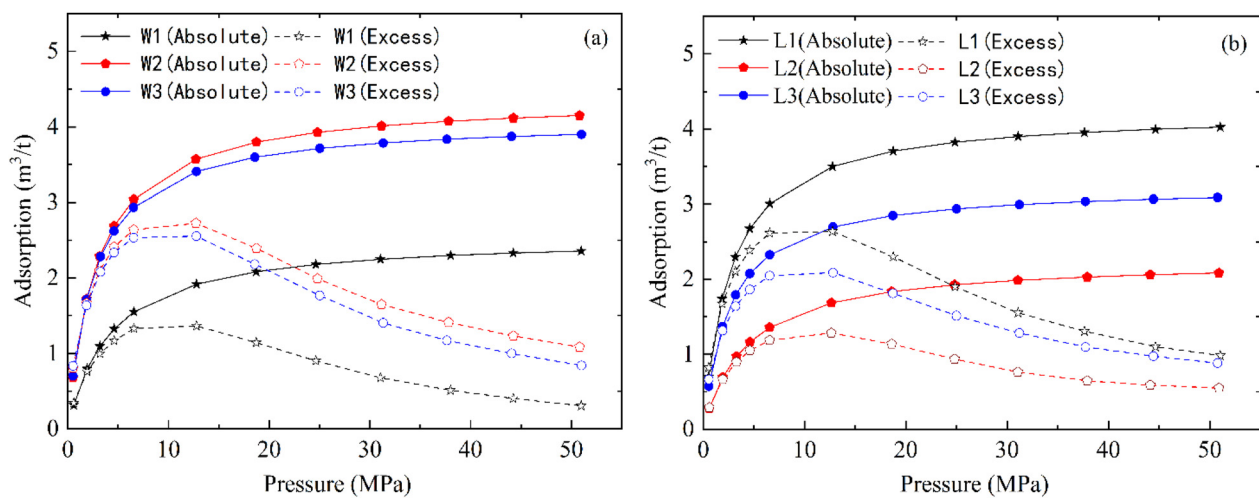


FIG. 5. Absolute and excess adsorption on deep shales at 313 K: (a) absolute and excess adsorption on W1–W3 and (b) absolute and excess adsorption on L1–L3.

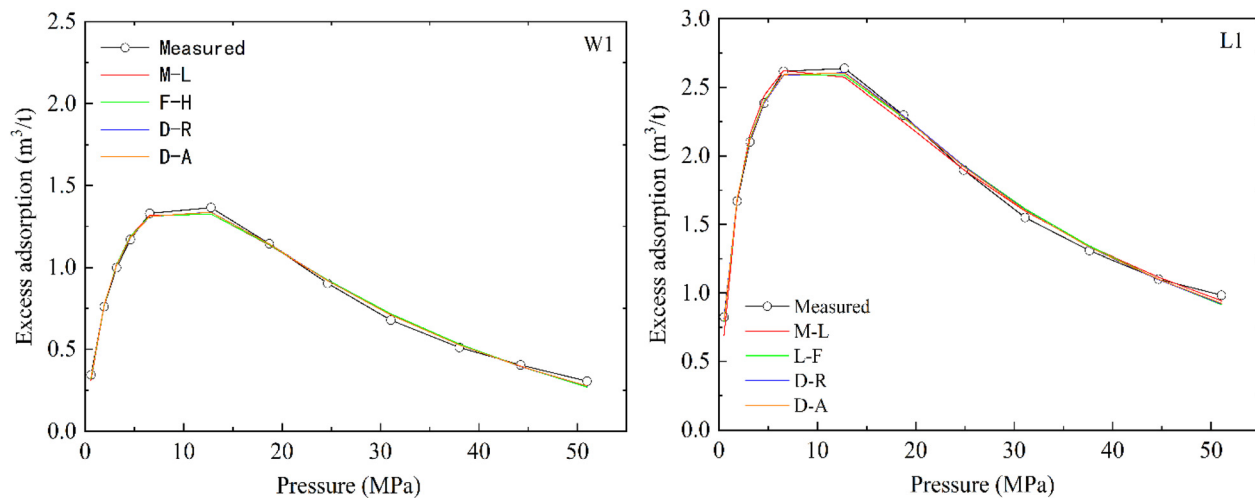


FIG. 6. Measured data and fitted adsorption models on deep shales.

studies.³⁶ This is consistent with the result that the micro- and nanopores of shales are more developed in the deep shale gas formations. Moreover, the ARE values of these adsorption models fitted at the low pressure (0–15 MPa) were obviously smaller than those at the high pressure (15–55 MPa), which implied that the methane molecule adsorption on shales would more complicated under the high-pressure condition.

D. Effect of temperatures and clay minerals on methane adsorption

The excess and absolute adsorption curves of methane on the deep shale samples at 313 and 333 K are illustrated in Fig. 7. As can be seen from Fig. 7, the effect of temperatures on the amount of methane adsorbed on deep shales varied similarly. When the pressure became lower than 20 MPa, the excess adsorption of methane on deep shales decreased as the increasing temperature, whereas the opposite trend would occur once the pressure exceeded some value. This phenomenon was also mentioned in previous studies, and the main reason may be attributed to the differences between the adsorbed density of the adsorbed phase and that of the gas phase.¹³ By contrast, the absolute adsorption of methane decreased with the increasing temperature since adsorption is an exothermic process, and the adsorption capacity increased rapidly below 10 MPa and the adsorption gas increased slowly until the equilibrium with the increasing pressure beyond

10 MPa. In addition, when the methane molecules were adsorbed on the shale surface, there existed two kinds of molecular interactions: adsorbate/adsorbate and adsorbent/adsorbate, which would affect the adsorption capacity on shales. It was mentioned that the adsorbate/adsorbate interaction could have been neglected in the previous studies.^{13,25} The discrepancy with the measured data implied that the adsorbate/adsorbate interaction would greatly affect the methane adsorption capacity. Otherwise, the increasing temperature could raise the methane adsorption process and result in a greater ratio of free gas molecules. Some weak adsorption sites could miss the methane molecules with the increasing temperature due to the heterogeneity distribution in the shale surface.⁴⁴ Consequently, the absolute adsorption of methane on deep shales decreased as the temperature increased.

The clay minerals have been widely considered as a crucial factor affecting the methane sorption capacity on shale rocks.⁴⁵ In order to understand the clay dependence of the methane adsorption capacity on deep shale samples, the maximum adsorption capacity at 313 K was plotted against the total clay content illustrated in Fig. 8. As can be seen from Fig. 8, the adsorption capacity of methane on shale samples was inversely correlated with the total content of clay minerals except for the W2, and this result was consistent with some previous studies on the marine shale rocks.^{45,46} This phenomenon may be resulting from the strong effect of TOC content as mentioned above. The adsorption capacity of methane on the clay-rich rocks was in the descending order of montmorillonite, illite/smectite mixed layer,

TABLE III. Average relative errors between measured data and adsorption models fitted.

Model	W1 (ARE, %)			L1 (ARE, %)		
	0–15 MPa	15–55 MPa	0–55 MPa	0–15 MPa	15–55 MPa	0–55 MPa
M-L	1.58	4.25	3.04	4.01	2.22	3.11
L-F	1.64	4.51	3.21	1.55	2.74	2.14
D-R	1.44	3.66	2.65	0.94	2.38	1.66
D-A	1.46	3.81	2.76	1.28	2.22	1.75

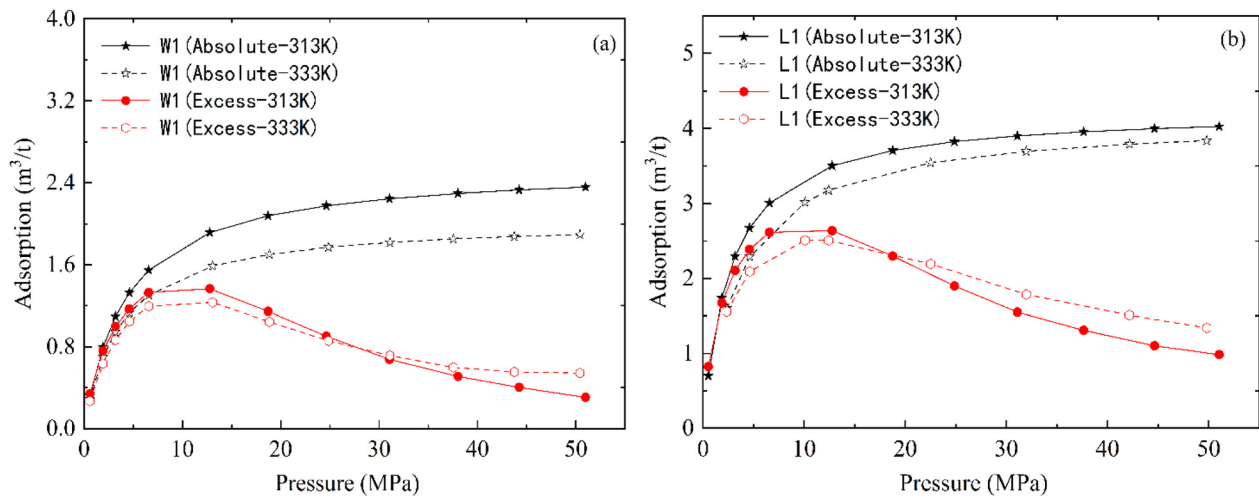


FIG. 7. Effect of temperatures on absolute and excess adsorption for deep shales: (a) deep shale W1 and (b) deep shale L1.

kaolinite, chlorite, and illite.⁴⁷ Among shales W1, W2, and W3, shale W2 showed the highest capacity of methane adsorption while shale W1 exhibited the lowest adsorption capacity. In this study, kaolinite, chlorite, and illite commonly existed in these deep shales, and resulted in methane adsorption capacity that decreased with clay minerals. Therefore, the methane adsorption behaviors on the deep shales were very closely related to the mineralogy and physicochemical structure and were more complex.

E. Effect of moisture on methane adsorption

The adsorption capacity of methane on the organic-rich shales could be greatly reduced due to the existence of the moisture content, and the moisture was able to occupy the adsorption sites in the shale pores.^{48,49} The excess adsorption curves of methane on the deep shale samples under dry and wet conditions are shown in Fig. 9. As can be seen from Fig. 9, the effect of moisture on the amount of methane adsorbed on these deep shales exhibited fairly similar characteristics.

When the temperature was constant, the excess adsorption capacity of methane on the deep shales under the wet condition decreased significantly at the same pressure, and the whole adsorption isotherms moved down compared with that in the dry condition. In the low-pressure stage, the excess adsorption isotherms increased rapidly and showed a nearly linear growth. When the adsorption entered the high-pressure stage (more than 13 MPa), the methane molecules in the adsorption layer gradually increased to the maximum adsorption capacity, and then the excess adsorption capacity gradually decreased with the increasing pressure. The moisture content of shale would greatly reduce the methane adsorption capacity, and the main reason was that water molecules would occupy adsorption sites in the shales, which resulted in the decrease in adsorption sites for methane molecules. Consequently, the effect of moisture on methane adsorption implies that the moisture content should be considered to estimate the methane adsorption capacity in shale gas reservoirs.

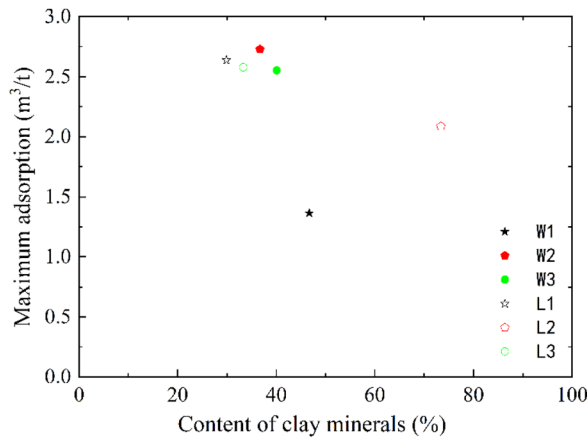


FIG. 8. Maximum adsorption capacity at 313 K vs clay minerals.

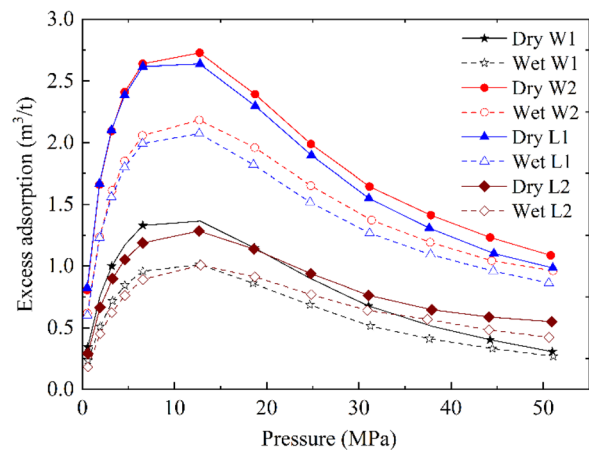


FIG. 9. Effect of moisture on excess adsorption for deep shales.

V. CONCLUSIONS

In this work, the high-pressure (up to 50 MPa) methane adsorption isotherms at different temperatures were measured on deep shales collected from the lower Silurian Longmaxi formation in the Sichuan Basin, South China. The high-pressure methane adsorption characteristics on deep shales were analyzed, and then the adsorption models were used to describe the methane adsorption behavior. Moreover, the effects of temperatures and clay minerals as well as moisture content on the methane adsorption capacity were discussed. According to the above results, the main conclusions from this study are summarized as follows: (1) The excess adsorption isotherms of methane on deep shales increased with pressures, then gradually reached their peak and finally decreased with the increasing of pressures beyond 13 MPa. The maximum excess adsorption capacities at pressures up to 50 MPa and 313 K on these deep shales were between 1.36 and 2.73 m³/t. The methane absolute adsorption amount on deep shales was a rapid increase trend and then a slight change trend with increasing pressures, which exhibited Type I isotherms. (2) The maximum excess adsorbed amounts on the deep shales were good linear positive correlations with the TOC content, and it had a significant effect on the methane sorption capacity, which implied that organic matter was the main carrier of methane molecules adsorbed in shales. Compared with these adsorption models, the D-R adsorption model provided the best fit to the experimental data at the entire pressure, which could describe and predict the high-pressure excess adsorption of methane on deep shales. (3) As the temperature increased, the excess adsorption of methane on deep shales decreased at some pressure, while the opposite trend would occur once it exceeded this pressure. Kaoline, chlorite, and illite commonly existed in these deep shales and brought about the methane adsorption capacity that decreased with clay minerals. (4) The presence of the moisture content on deep shales sharply decreased the methane adsorption capacities. As the increasing pressure, the effect of moisture content on methane adsorption in shales decreased and then maintained stable. The moisture could occupy the adsorption sites in shale pores, which resulted in the methane adsorption capacity that decreased with moisture.

ACKNOWLEDGMENTS

This work was supported by the National Natural Science Foundation of China (Grant Nos. 11802312 and U1762216), and by the Open Fund (PLN201810) of State Key Laboratory of Oil and Gas Reservoir Geology and Exploitation (Southwest Petroleum University).

DATA AVAILABILITY

The data that support the findings of this study are available from the corresponding author upon reasonable request.

REFERENCES

- W. J. Zhang, W. Chen, T. X. Wang *et al.*, "A self-similarity mathematical model of carbon isotopic flow fractionation during shale gas desorption," *Phys. Fluids* **31**(11), 112005 (2019).
- Z. H. Xu, M. J. Zheng, Z. H. Liu *et al.*, "Petrophysical properties of deep Longmaxi formation shales in the southern Sichuan basin, SW China," *Pet. Explor. Dev.* **47**(6), 1183–1193 (2020).
- X. Z. Li, Z. H. Guo, Y. Hu *et al.*, "High-quality development of ultra-deep large gas fields in China: Challenges, strategies and proposals," *Nat. Gas Ind.* **7**(5), 505–513 (2020).
- X. H. Ma, J. Xie, R. Yong *et al.*, "Geological characteristics and high production control factors of shale gas reservoirs in Silurian Longmaxi formation, southern Sichuan basin, SW China," *Pet. Explor. Dev.* **47**(5), 901–915 (2020).
- W. J. Shen, L. G. Zheng, C. M. Oldenberg *et al.*, "Methane adsorption and diffusion in shale rocks: A numerical study using the dusty gas model in TOUGH₂/EOS-C-ECBM," *Transp. Porous Media* **123**(3), 521–531 (2018).
- Y. Xia, J. Goral, H. Huang *et al.*, "Many-body dissipative particle dynamics modeling of fluid flow in fine-grained nanoporous shales," *Phys. Fluids* **29**(5), 056601 (2017).
- P. Whitelaw, C. N. Uguna, L. A. Stevens *et al.*, "Shale gas reserve evaluation by laboratory pyrolysis and gas holding capacity consistent with field data," *Nat. Commun.* **10**, 3659 (2019).
- L. Germanou, M. T. Ho, Y. H. Zhang *et al.*, "Shale gas permeability upscaling from the pore-scale," *Phys. Fluids* **32**(10), 102012 (2020).
- X. H. Ma, W. J. Shen, X. Z. Li *et al.*, "Experimental investigation on water adsorption and desorption isotherms of the Longmaxi shale in the Sichuan basin, China," *Sci. Rep.* **10**, 13434 (2020).
- R. J. Ambrose, R. C. Hartman, M. Diaz-Campo *et al.*, "Shale gas-in-place calculations part I: New pore-scale considerations," *SPE J.* **17**(1), 219–229 (2012).
- T. F. T. Rexer, M. J. Benham, A. C. Aplin *et al.*, "Methane adsorption on shale under simulated geological temperature and pressure conditions," *Energy Fuels* **27**(6), 3099–3109 (2013).
- A. Merkel, R. Fink, and R. Littke, "High pressure methane sorption characteristics of lacustrine shales from the Midland Valley basin, Scotland," *Fuel* **182**, 361–372 (2016).
- Z. Jiang, L. Zhao, and D. X. Zhang, "Study of adsorption behavior in shale reservoirs under high pressure," *J. Nat. Gas Sci. Eng.* **49**, 275–285 (2018).
- L. Wang, J. M. Wan, T. K. Tokunaga *et al.*, "Experimental and modeling study of methane adsorption onto partially saturated shales," *Water Resour. Res.* **54**(7), 5017–5029, <https://doi.org/10.1029/2017WR020826> (2018).
- R. R. Qi, Z. F. Ning, Q. Wang *et al.*, "Measurements and modeling of high-pressure adsorption of CH₄ and CO₂ on shales," *Fuel* **242**, 728–743 (2019).
- K. Hu and H. Mischo, "Modeling high-pressure methane adsorption on shales with a simplified local density model," *ACS Omega* **5**, 5048–5060 (2020).
- B. Hou, Z. Chang, W. Fu *et al.*, "Fracture initiation and propagation in a deep shale gas reservoir subject to an alternating-fluid-injection hydraulic-fracturing treatment," *SPE J.* **24**(4), 1839–1855 (2019).
- W. Yu, K. Sepehrnoori, and T. W. Patzek, "Modeling gas adsorption in Marcellus shale with Langmuir and BET isotherms," *SPE J.* **21**(2), 589–600 (2016).
- H. Tian, T. F. Li, T. W. Zhang *et al.*, "Characterization of methane adsorption on overmature lower Silurian-upper Ordovician shales in Sichuan basin, southwest China: Experimental results and geological implications," *Int. J. Coal Geol.* **156**, 36–49 (2016).
- X. Song, X. X. Lü, Y. Q. Shen *et al.*, "A modified supercritical Dubinin-Radushkevich model for the accurate estimation of high pressure methane adsorption on shales," *Int. J. Coal Geol.* **193**, 1–15 (2018).
- W. Tian and H. Q. Liu, "Insight into the adsorption of methane on gas shales and the induced shale swelling," *ACS Omega* **5**(49), 31508–31517 (2020).
- S. W. Zhou, Y. Ning, Y. H. Y. Wang *et al.*, "Investigation of methane adsorption mechanism on Longmaxi shale by combining the micropore filling and monolayer coverage theories," *Adv. Geo-Energy Res.* **2**(3), 269–281 (2018).
- M. N. Nounou and H. N. Nounou, "Multiscale estimation of the Freundlich adsorption isotherm," *Int. J. Environ. Sci. Technol.* **7**(3), 509–518 (2010).
- P. Chareonsuppanimit, S. A. Mohammad, R. L. Robinson *et al.*, "High-pressure adsorption of gases on shales: Measurements and modeling," *Int. J. Coal Geol.* **95**, 34–46 (2012).
- X. Tang, N. Ripepi, K. Luxbacher *et al.*, "Adsorption models for methane in shales: Review, comparison, and application," *Energy Fuels* **31**(10), 10787–10801 (2017).
- H. Li, B. B. Li, C. H. Ren *et al.*, "An adsorption model for evaluating methane adsorption capacity in shale under various pressures and moisture," *J. Nat. Gas Sci. Eng.* **81**, 103426 (2020).
- S. B. Chen, Y. M. Zhu, Y. Qin *et al.*, "Reservoir evaluation of the lower Silurian Longmaxi formation shale gas in the southern Sichuan basin of China," *Mar. Pet. Geol.* **57**(2), 619–630 (2014).

- ²⁸S. Brunauer, P. H. Emmett, and E. Teller, "Adsorption of gases in multimolecular layers," *J. Am. Chem. Soc.* **60**, 309 (1938).
- ²⁹B. C. Lippens and J. H. de Boer, "Studies on pore systems in catalysts: V. The t method," *J. Catal.* **4**, 319 (1965).
- ³⁰M. D. Donohue and G. L. Aranovich, "Classification of Gibbs adsorption isotherms," *Adv. Colloid Interface Sci.* **76–77**, 137–152 (1998).
- ³¹L. Hamon, L. Chenoy, and G. Weireld, "Determination of absolute gas adsorption isotherms: Simple method based on the potential theory for buoyancy effect correction of pure gas and gas mixtures adsorption," *Adsorption* **20**(2–3), 397–408 (2014).
- ³²G. Soave, "Equilibrium constants from a modified Redlich–Kwong equation of state," *Chem. Eng. Sci.* **27**, 1197–1203 (1972).
- ³³R. S. Myong, "Gaseous slip models based on the Langmuir adsorption isotherm," *Phys. Fluids* **16**(1), 104–117 (2004).
- ³⁴R. Sip, "On the structure of a catalyst surface," *J. Chem. Phys.* **16**, 490–495 (1948).
- ³⁵M. M. Dubinin, "Adsorption in micropores," *J. Colloid Interface Sci.* **23**, 487–499 (1967).
- ³⁶R. Sakurovs, S. Day, A. S. Weir *et al.*, "Application of a modified Dubinin–Radushkevich equation to adsorption of gases by coals under supercritical conditions," *Energy Fuel* **21**, 992–997 (2007).
- ³⁷M. M. Dubinin and V. A. Astakhov, "Development of the concepts of volume filling of micropores in the adsorption of gases and vapors by micro-porous adsorbents," *Bull. Acad. Sci. USSR, Div. Chem. Sci. (Engl. Transl.)* **20**, 3–7 (1971).
- ³⁸C. Boyer, J. Kieschnick, R. Suarez-Rivera *et al.*, "Producing gas from its source," *Oilfield Rev.* **18**(3), 36–49 (2006); available at <https://www.discoverygeo.com/resources/Papers/Great-Article-on-Geochemistry.pdf>.
- ³⁹W. J. Shen, X. Z. Li, A. Cihan *et al.*, "Experimental and numerical simulation of water adsorption and diffusion in shale gas reservoir rocks," *Adv. Geo-Eng. Res.* **3**(2), 164–175 (2019).
- ⁴⁰F. Yang, Z. F. Ning, and H. Q. Liu, "Fractal characteristics of shales from a shale gas reservoir in the Sichuan basin, China," *Fuel* **115**, 378–384 (2014).
- ⁴¹J. Xiong, X. J. Liu, L. X. Liang *et al.*, "Methane adsorption on carbon models of the organic matter of organic-rich shales," *Energy Fuel* **31**, 1489–1501 (2017).
- ⁴²X. Tang, N. Ripepi, N. P. Stadie *et al.*, "A dual-site Langmuir equation for accurate estimation of high pressure deep shale gas resources," *Fuel* **185**, 10–17 (2016).
- ⁴³J. W. Liu, P. C. Li, Z. Y. Sun *et al.*, "A new method for analysis of dual pore size distributions in shale using nitrogen adsorption measurements," *Fuel* **210**, 446–454 (2017).
- ⁴⁴Z. H. Ye, D. Chen, Z. J. Pan *et al.*, "An improved Langmuir model for evaluating methane adsorption capacity in shale under various pressures and temperatures," *J. Nat. Gas Sci. Eng.* **31**, 658–680 (2016).
- ⁴⁵M. Gasparik, A. Ghanizadeh, P. Bertier *et al.*, "High-pressure methane sorption isotherms of black shales from The Netherlands," *Energy Fuels* **26**(8), 4995–5004 (2012).
- ⁴⁶J. Q. Tan, P. Weniger, B. Krooss *et al.*, "Shale gas potential of the major marine shale formations in the upper Yangtze platform, South China, Part II: Methane sorption capacity," *Fuel* **129**, 204–218 (2014).
- ⁴⁷L. M. Ji, T. W. Zhang, K. L. Milliken *et al.*, "Experimental investigation of main controls to methane adsorption in clay-rich rocks," *Appl. Geochem.* **27**(12), 2533–2545 (2012).
- ⁴⁸J. Zou, R. Rezaee, Q. Xie *et al.*, "Investigation of moisture effect on methane adsorption capacity of shale samples," *Fuel* **232**, 323–332 (2018).
- ⁴⁹T. Zhao, X. F. Li, H. W. Zhao *et al.*, "Molecular simulation of adsorption and thermodynamic properties on type II kerogen: Influence of maturity and moisture content," *Fuel* **190**, 198–207 (2017).